SPE-209987-MS

Assessing the Underground Hydrogen Storage Potential of Depleted Gas Fields in Northern California

Esuru Rita Okoroafor, Tae Wook Kim, Negar Nazari, Hannah Yuh Watkins, Sarah D. Saltzer, and Anthony R. Kovscek, Stanford University

This paper was prepared for presentation at the 2022 SPE Annual Technical Conference and Exhibition held in Houston, Texas, USA, 3 - 5 October 2022.

Abstract

The goal of this study was to assess the potential for storing hydrogen underground in depleted gas fields in Northern California. We considered the potential amount of hydrogen generated from the electrolysis of California's curtailed solar and wind energy. We then determined the fields with the best geological and reservoir properties to support secure underground hydrogen storage.

We developed a three-stage set of criteria for selecting potential hydrogen storage sites. In stage 1, our screening approach combines integrated geoscience and environmental factors to identify the fields to exclude from consideration for hydrogen storage. In stage 2, we applied a numerical simulation-based site selection criteria to the fields that passed the stage 1 screening criteria. We started the screening with 182 depleted and underground storage fields in Northern California, of which 147 fields were disqualified in the first stage. We scored and ranked the remaining 35 fields based on their potential to maximize storage and withdrawal of hydrogen using the numerical simulation-based site selection criteria. The top-ten high scoring sites for underground hydrogen storage and production were reservoirs with dips between 5° and 15°, reservoir porosity above 20%, reservoir flow capacity above 5000 mDm, and reservoirs at depths between 430 m to 2400 m. The total estimated hydrogen storage capacity for the ten high-scoring sites was 203.5 million tonnes of hydrogen. Our set of site selection criteria has a stage 3 that requires detailed site characterization. With stage 3, we gather additional rock and fluid properties of high-scoring sites that enable detailed modeling of the processes related to hydrogen storage and withdrawal. We did not cover stage 3 in this paper.

We estimated the potential hydrogen recovery from a hypothetical depleted field in California and evaluated the efficiency of converting the renewable energy to hydrogen and back to power. The results show that depleted gas fields in Northern California have sufficient storage capacity to support the seasonal underground storage of hydrogen derived from renewable energy electrolysis. However, recovery is limited to the amount of fluid that can be injected, the mixing between hydrogen and the *in-situ* gas, and the lateral spread of hydrogen. The round-trip efficiency of power to hydrogen to power conversion maxed at 36% for the system under study.

Introduction

Global warming and climate change have been attributed to increased anthropogenic greenhouse gas (GHG) emissions since the pre-industrial era (Ritchie et al., 2020). Several strategies to reduce greenhouse gas emissions include energy efficiency, energy conservation, changes to land use and land use management practices, carbon capture and sequestration, and fuel switching. Fuel switching in the electricity and power sector may involve a shift toward low-carbon electricity, such as renewable energy resources, nuclear energy, or shifting from coal or petroleum to natural gas. Fuel switching for sectors such as transport may involve electrifying transportation or using a fuel with zero or low carbon emissions.

Hydrogen is a core sector resource inherent in fuel switching and energy storage. Hydrogen is poised to contribute significantly to meeting net-zero emission targets and decarbonization. It can be used as an energy carrier for electricity generation, can be used as a fuel to decarbonize difficult sectors such as industry, and can be used in fuel cells to decarbonize the transport sector. Hydrogen does not exist freely in nature and needs to be produced or generated from different sources. Figure 1 shows possible pathways to generate hydrogen from various energy resources, how hydrogen can be stored, and how it can be utilized. Producing hydrogen from natural gas using Steam Methane Reforming (SMR) is the most common and economical way to produce hydrogen (Bracci, et al., 2022), amounting to about 80% of the hydrogen produced in the US and 40% in the world (DOE/NETL, 2010). The SMR process, however, emits CO_2 at 9.7 kg CO_2/kg H_2 (Scholz, 1993).

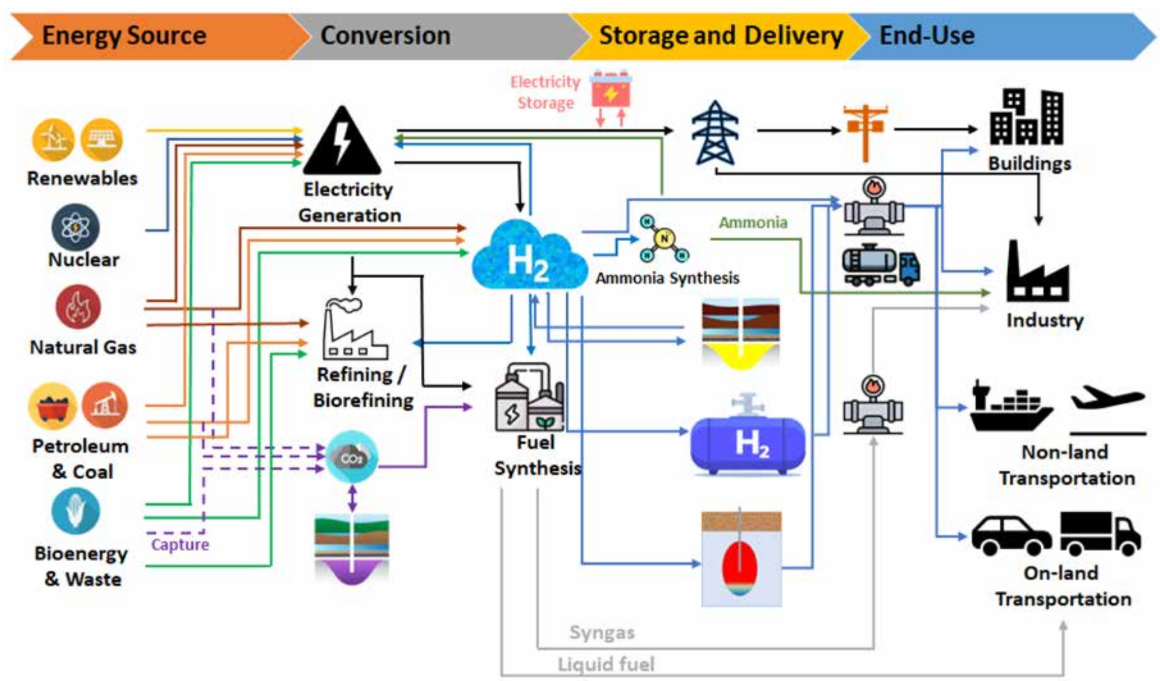

Figure 1—Hydrogen generation value chain. Dashed lines indicate a possibility of CO_2 capture with the hydrogen production process to reduce CO_2 emissions.

Renewable energy resources such as solar and wind provide emission-free electricity (not including life cycle effects). These renewable resources are seasonal and generate electricity intermittently. Excess electricity produced from these resources can be converted to hydrogen using electrolysis, where water is split into hydrogen and oxygen.

The hydrogen can be stored and later converted to electricity to power the grid as needed. Hydrogen can be stored using different technologies. These include compressed gas vessels, metal hydrides, complex hydrides, chemical hydrides (such as methanol, ammonia, and formic acid), hydrogen sorbents, liquid organic hydrogen carriers, pipeline storage, and underground hydrogen storage in geological media (Stetson et al., 2016; Panfilov, 2016; Andersson & Grönkvist, 2019). Underground hydrogen storage in geological media has been identified as economical for storing large amounts of hydrogen that could complement large-scale energy storage (Panfilov, 2016). These underground geological media exist in the form of salt caverns and porous media, i.e., saline aquifers and depleted natural gas reservoirs. Salt caverns are frequently used to store natural gas. Hydrogen storage in salt caverns is already practiced in the United States, Britain, and Germany (Zivar et al., 2020). Unfortunately, salt structures have restricted cavern volume (compared to a saline aquifer) and geographical limitations in the occurrence of salt deposits suitable for salt-leached cavern construction.

Saline aquifers and depleted gas reservoirs, compared to salt caverns, can store much larger gas volumes and are widespread geographically. However, the hydrogen storage experience in these media is few, and a detailed understanding of the behavior of hydrogen in porous media is in the research and early field development stages. Depleted gas reservoirs are low-hanging fruit for underground hydrogen storage compared to other porous media. Depleted gas reservoirs are characterized adequately for geological and reservoir properties. In addition, there is experience with underground gas storage in depleted reservoirs, as 75% of underground gas storage (UGS) sites in the world are in depleted hydrocarbon fields (Tarkowski, 2019). Moreover, if hydrogen is burned in gas-fired turbines or injected into natural gas pipelines, the presence of natural gas in the reservoir will not be a challenge for the purity of the stored hydrogen. Consequently, this work demonstrates the application of a novel and comprehensive site screening and selection criteria for underground hydrogen storage in porous media. The interdisciplinary approach highlights the critical role of oil and gas professionals in hydrogen storage as a complement to solar and wind energy resources.

Study Motivation

California has made great strides in its transition to a low-carbon electricity grid. The increase in solar and wind resources has led to a new paradigm, in which there are certain times of the day and seasons when there is an oversupply of renewable energy generation and not enough demand to use them. Currently, the most effective tool of California's Independent System Operator (CAISO) for managing oversupply is to curtail renewable resources. That means reducing the output of renewable generators below what it could have otherwise produced.

To help meet California's target of 50% renewable generation by 2025, additional renewable capacity needs to be added to the grid. While the additional renewable capacity will increase renewable energy generation, it is anticipated that the curtailment of solar and wind will increase (EIA, 2021). In addition, residential solar generation has continued to grow, decreasing the need for CAISO-operated generation and leading to further solar curtailments.

To this end, CAISO has been exploring and implementing various solutions to manage curtailment (California ISO, 2022), including CAISO's Energy Imbalance Market (EIM) and battery storage. Hydrogen production and hydrogen-based energy storage could also help reduce solar curtailments. The current curtailment solutions may not be sufficient to address the increasing curtailment. For example, in 2020, only 16% of total possible curtailments were avoided by trade within the EIM. Similarly, the use of hydrogen tanks in hydrogen-based energy storage is small compared to the amount of energy being curtailed. Hence, hydrogen storage in subsurface geological formations presents itself as a possible solution to manage curtailment due to the large capacity and abundance of subsurface reservoirs in California.

Study Objectives

The objectives of this study are twofold. The first is to identify locations in California that are potentially suitable for storing hydrogen in the subsurface. The second is to determine the overall power-to-hydrogen-to-power efficiency, assuming a combined cycle gas turbine will be used to generate power.

Scope of study and organization of the paper

In this study, we focus on depleted fields in Northern California as potential storage sites for curtailed energy. We consider flow dynamics in the section on numerical simulation, but do not consider geochemical reactions, geomechanical effects and microbial activity in the subsurface. The organization of the paper is as follows. First, we describe the data sources and how they can be used to high-grade storage sites suitable for hydrogen storage. This is followed by estimating the amount of hydrogen that needs to be stored from the curtailed energy. We then apply the site selection criteria to screen and rank the fields. Finally, we estimate the round-trip power-to-hydrogen-to-power efficiency.

Methods

Data on Northern California Depleted Gas Fields

California has 516 oil & gas fields in 4 different districts (Northern, Inland, Coastal, and Southern districts) (CA DOC, 2022). In the northern district, there are 175 oil and gas fields, and 7 underground gas storage (UGS) sites (CA DOC, 2022). To screen and qualify each field, geological properties, geological structure, and risk-induced data were prepared using existing references and public data. The California Division of Oil, Gas and California Geothermal Resources (CA DOGGR, also called the California Department of Conservation (CA DOC)) published geological properties, conditions (pressure and temperature), structure, operation history, and salinity for each oil and gas field (CA DOGGR, 1982). Regarding UGS fields, the California Council on Science and Technology (CA CST) reported and summarized properties for underground structures (Long et al., 2019). The estimated CO2 storage resource in oil and gas fields from the National Carbon Sequestration Database and Geographic Information System's (NATCARB) study (NETL, 2015) was used to calculate the H2 storage resource, although the density of hydrogen at 30 bar and 40 °C was used in place of the CO_2 density.

CA DOC made available in public database information about wells in California, including well log, production, injection, areal location, and permitting documentation to understand the current geological conditions in each field (CA DOC, 2022). Porosity data was available for all sites, while permeability data was scarce. Hence, we used a porosity-permeability transform to estimate permeability for the fields. The Environmental Protection Agency (EPA) Emission & Generation Resource Integrated Database (eGRID) was used to locate the wind and solar farms (US EPA, 2022). The database provided global positioning system (GPS) information, the number of units, and capacity.

In addition, the exclusion zones defined to eliminate hydrogen injection sites, based on factors such as proximity to geological faults, were identical to the previous study that discussed the exclusion zones for CO2 storage sites (Kim et al., 2022a). Detailed descriptions and references are available in a prior study (Kim et al., 2022a, Kim et al., 2022b). The quaternary faults and active seismic areas were eliminated in the active fields due to potential risk. Regarding non-active fields, additional exclusion zones, including high population density, restricted lands, and sensitive zones, were considered.

Estimating the storage capacity needed

Increasing renewable curtailments of solar and wind in California opens new opportunities toward storing renewable energy for later use. Evaluating surplus and curtailed energy reveals that renewable resources in California may generate more electricity than is needed, especially in the middle of the day. Figure 2 shows an increasing trend in California's wind and solar curtailment between 2014 and 2021. The maximum curtailment happens from February to May. Storing the curtailed energy from wind and solar provides an opportunity to use the energy in the later months.

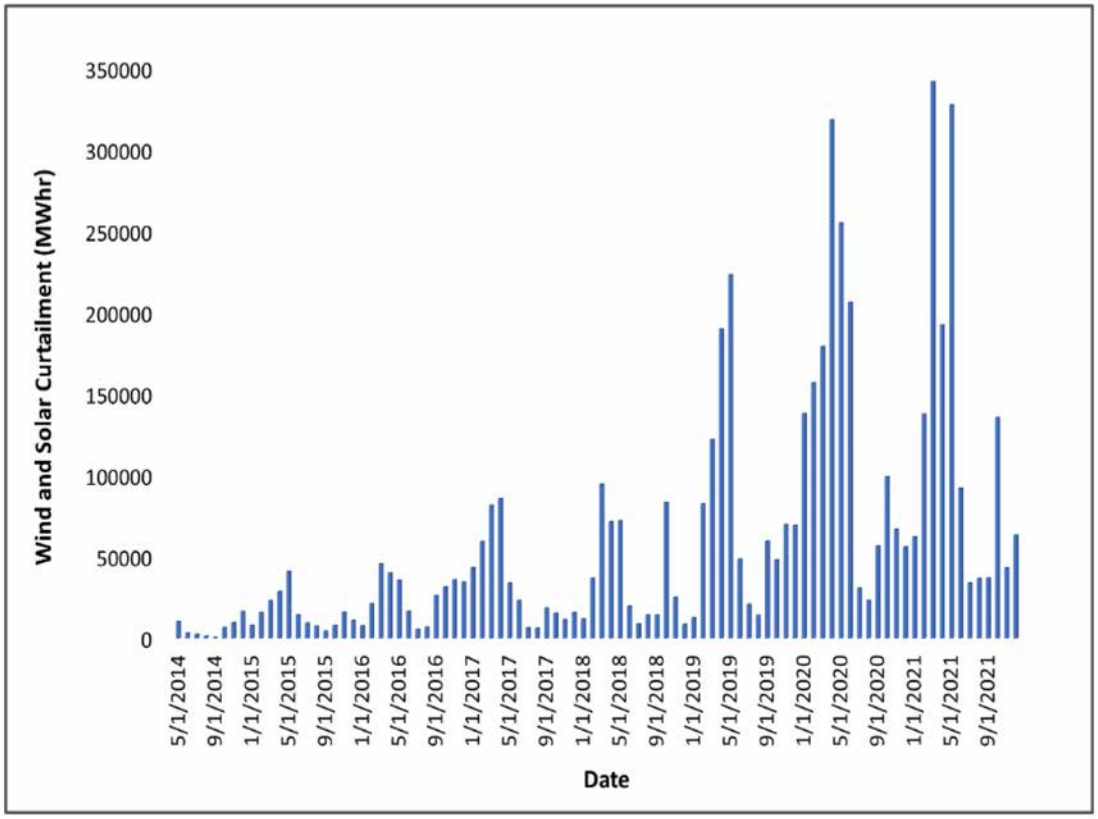

Figure 2—Wind and solar curtailment in MWh for the state of California from 2014 through 2021 (California ISO, 2022).

One storage method is to produce hydrogen from surplus renewable electricity and store it for later use. Among various sources for the commercial production of hydrogen (including natural gas, oil, coal, and electrolysis), electrolysis accounts for 4% of the world's hydrogen production (Press et al. 2008).

There are four types of electrolyzers: Alkaline, Polymer Electrolyte Membrane (PEM), Anion Exchange Membrane (AEM), and Solid Oxide. Alkaline and PEM are already commercial, while AEM and solid oxide currently exist at lab scale. The electrolyzer technologies are different in critical materials to performance, durability, and maturity. We conducted this study based upon PEM electrolyzer performance. PEM systems are much simpler than alkaline and have more design choices including atmospheric, differential, and balanced pressure. Their membrane electrolyte operates under differential pressure, typically 30 bar to 70 bar, and temperatures of 50-80 °C (IRENA, 2020). In addition, compared to alkaline electrolysis, PEM electrolysis has the advantage of quickly reacting to the fluctuations typical of renewable power generation. The technology is often used for distributed systems because the equipment is low-maintenance and delivers high-quality gas (Lichner, 2020). PEM electrolyzers have efficiencies in the range of 50-83 kWh/kgH_2. Therefore, we converted the curtailed wind and solar energy into mass of hydrogen using the upper and lower bounds of the efficiencies mentioned above. Subsequently, we used the hydrogen density at 15.6 °C and 1 atm (0.08504 kg/m^3) to convert the hydrogen mass (kg) into hydrogen volume (m^3).

Defining the storage cycle

The storage cycle is defined based on the solar and wind curtailment periods. From the trend in Fig. 2, we observed that the amount of curtailment reaches a maximum between February to May. Then, it decreases for the three following months (June through August). We observe another peak in the year's final months (September to December). Therefore, we defined our cycles according to these fluctuations and variations, such that we will store hydrogen for the first peak of the year (February through May), withdraw for the second period (June through August), store hydrogen again for the final peak period (September through December), and make the final withdrawal in January of the year that follows.

Site selection criteria used

Description of the site selection criteria. The underground hydrogen storage site selection criteria are a set of methodologies used to determine a site, or sites, that best meet established requirements (e.g., sufficient capacity and injectivity, low leakage or induced seismicity risk, and low costs) to support the storage of hydrogen in the subsurface. The methodology modifies a selection process similar to Callas et al. (2022). Site selection is divided into three stages: site screening, site ranking, and site characterization. Figure 3 summarizes the site selection workflow proposed by Callas et al. to select the most suitable CO_2 site(s) from a pool of potential input sites. The workflow utilizes information generally available in public databases, geological surveys, or storage atlases for the site screening and ranking stages. Additional information, simulations, and data may need to be acquired or performed to select the optimal site in the site characterization stage. The data required at each stage and the complexity of analysis increase while the number of sites evaluated decreases.

1. *Site Screening* is the first stage many potential sites are eliminated because they do not meet a qualifying threshold based on capacity, productivity, injectivity, geological, economic, and siting considerations. The sites that meet these qualifying criteria move to Stage 2, site ranking.
2. *Site Ranking* scores and ranks the sites that met the thresholds in the site-screening stage. These sites receive a normalized score between one and five for every criterion. Each site receives a technical score that combines the capacity and injectivity optimization and retention and geomechanical risk minimization criteria scores, a siting and economic constraints score, and a combined overall score. The user assigns a weight to each criterion based on the most important parameters for their project. The highest-ranking sites move onto the site characterization stage.
3. *Site Characterization* is the final stage where the top-ranking sites from Stage 2 are analyzed in detail so that the user determines the most suitable site(s). Additional data may need to be acquired at this stage (e.g., seismic, pilot test data), or computational and experimental studies may need to be performed to characterize each reservoir.

In this study, we only focused on Stage 1 and Stage 2 in accessing potential sites in northern California for underground hydrogen storage.

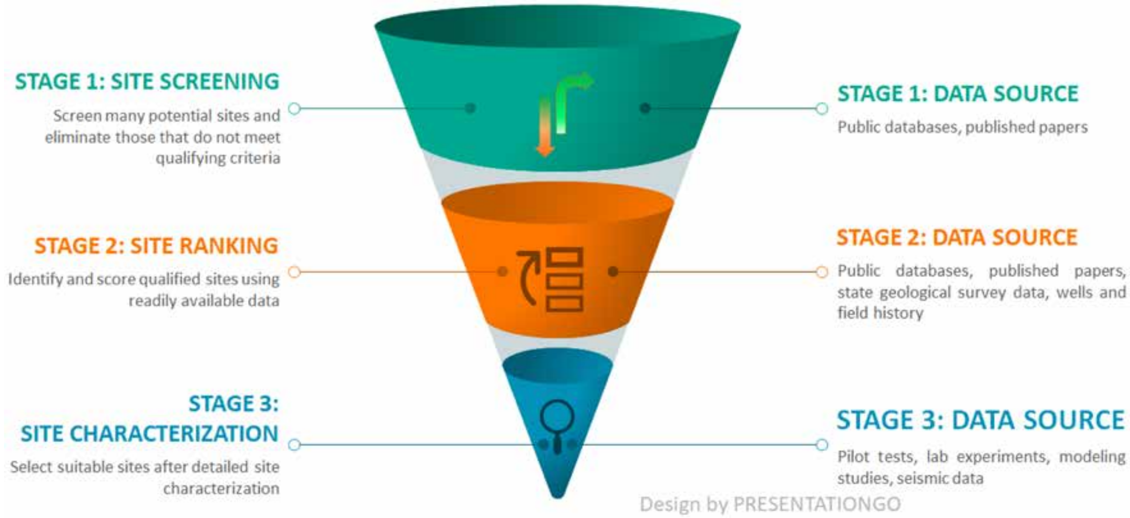

Figure 3—Overview of the site selection workflow designed to select the most suitable site from a pool of potential input sites taken from Callas et al. (2022).

Stage 1 and Stage 2 criteria. We used a numerical simulation-based site selection criteria developed by Okoroafor et al. (2022). The site selection criteria involved rigorous sensitivity analyses to understand the interplay of geological and reservoir engineering factors on hydrogen storage and withdrawal in depleted gas reservoirs. In addition, the site selection criteria are optimized for the energy required to compress hydrogen for storage in the subsurface. Table 1 shows the stage 1 screening criteria, while Table 2 shows the stage 2 scoring criteria. Detailed explanations for these criteria are available in Okoroafor et al. (2022). In Table 2, the permeability heterogeneity contrast is the ratio of permeability in the top layer to permeability in the layer that follows. The reservoir dip criterion in Table 2 assumes the well is placed updip of the structure.

Table 1—Proposed selection thresholds for hydrogen storage sites.

Category	Criteria	Disqualifying Threshold (metric units)
Storage and Withdrawal Optimization	Reservoir pressure (P_r)	Wellhead Pressure Constraint > P_r-(0.01 bar/m) × reservoir top depth (in meters)
	Maximum Depth of Formation Top	>3000 m
	Permeability	<50 mD
	Porosity	<10%
	Net Reservoir Thickness	<10 m
Risk and Hydrogen Loss Minimization	Top Seal Thickness	<20m
	Secondary Confining Units	No secondary confining units
	Active/Inactive Faulting	4 km wide "buffer zone" around all quaternary faults
	Earthquake Record	10 km diameter for M>5 (from 1769 – present), 5 km diameter for M<5 (from 2015 – present)
	Resources in the reservoir	Oil or Gas Condensate
Environmental and Economic Considerations	City Nearby	Within city boundaries
	Restricted lands	Within restricted lands
	Sensitive habitats	Within sensitive habitats
	Population density	Above 75 persons/ km^2
	Proximity to source or distribution point	> 30 km within source of hydrogen
	Access to existing pipelines or transport facilities	No access to existing pipelines or transport facilities
	Land ownership	Inability to secure land ownership for the project

Table 2—Proposed scoring criteria for underground hydrogen storage.

Criteria	1 (worst)	2	3	4	5 (best)
Permeability Thickness / Flow capacity (mDm)	<1000	1,000 - 10,000	10,000-40,000	>100,000	40,000-100,000
Size (Storage Capacity); Million tonnes of Hydrogen (MT H_2)	<1 MT	1-10 MT	10-50 MT	50-100 MT	> 100 MT
Permeability anisotropy	>0.8		0.5-0.8		0.1-0.5
Porosity (%)	<10		10-30		>30
Permeability Heterogeneity Contrast	<1		>1		1
Current Reservoir Pressure (bar)	>220	160 - 220	80 - 160	50 - 80	<50
Reservoir dip (degrees, °)		0-5	> 15	10-15	5-10
Reservoir Structure	Flat		Anticlinal / Moderately Dipping		Steeply Dipping
Geothermal Gradient (°C/km)	Warm Basin (>40)		Moderate (20-40)		Cold Basin (<20)

We developed an Excel-VBA tool to automate the site selection process based on the stage 1 and stage 2 site selection criteria. This was used to screen and rank the fields efficiently.

Weighting Factors

In the work by Okoroafor et al. (2022), a sensitivity analysis was performed to identify the parameters that had more impact on hydrogen productivity. The study showed that the dip angle, permeability, thickness, depth of the reservoir, and pressure of the reservoir had a significant impact on hydrogen productivity. Parameters including area, temperature gradient, and porosity had minimal impact on hydrogen productivity. While the area was not a significant parameter, the storage capacity (volume) is critical for underground gas storage. Based on these findings, we selected weighting factors to account for the significance of different parameters. The weighting factors used in this study are listed in the Table 3.

Table 3—Parameters used for scoring potential sites and their weighting factors.

Parameter	Unit	Weighting Factor
Flow capacity (Kh) = permeability * thickness	mDm	2
Dip angle	°	1.5
Reservoir Pressure	bar	1.5
Reservoir Structure	-	1.25
Reservoir Volume	Mt H_2	1.25
Geothermal Gradient	°C/km	1
Porosity	-	1

Numerical Simulation

To establish the amount of hydrogen that can be recovered after storage in a depleted gas reservoir, we used a numerical simulator to model the injection-withdrawal process. ECLIPSE E300, a multiphase-multicomponent simulation code, was used to run the reservoir simulation. The hypothetical numerical simulation model is a 2000 m by 2000 m reservoir with a spatial discretization of 20 m × 20 m in the lateral direction. The reservoir thickness is 40 m with a cell thickness of 5 m in the z-direction. The reservoir is flat with the top of the reservoir at a depth of 1000 m and is assumed to be closed at the top (sealing caprock) to prevent losses of hydrogen. The reservoir model parameters are provided in Table 4. Figure 3 shows the simulation domain.

Table 4—Parameters used in the model and other calculations related to this study.

Symbol	Description	Value	Units
φ	Porosity of the reservoir	0.28	-
k_H	Horizontal reservoir permeability	250	mD
k_V	Vertical reservoir permeability	50	mD
T_r	Average reservoir temperature	43	ºC
p_r	Average reservoir pressure	80	bar
GIP	Gas in place (methane)	4.69×10^9	Sm^3
c_r	Rock compressibility	1.01×10^{-4}	bar^{-1}
p_{ref}	Reference pressure for fluid density	1.013	bar
T_{ref}	Reference temperature for fluid density	15.56	ºC
ρ_f	Water density	999.7	kg/m^3
c_w	Water compressibility at reservoir conditions	2.0×10^{-4}	bar^{-1}
B_w	Water formation volume factor at reservoir conditions	1.1	m^3/Sm^3
μ_w	Water dynamic viscosity at reservoir conditions	0.62	cP

We determined the rock compressibility using Newman's correlation for consolidated sandstones (Newman, 1973) given by

$$c_f = \frac{97.3 \times 10^{-6}}{[1 + 55.9\varphi]^{1.429}} \tag{1}$$

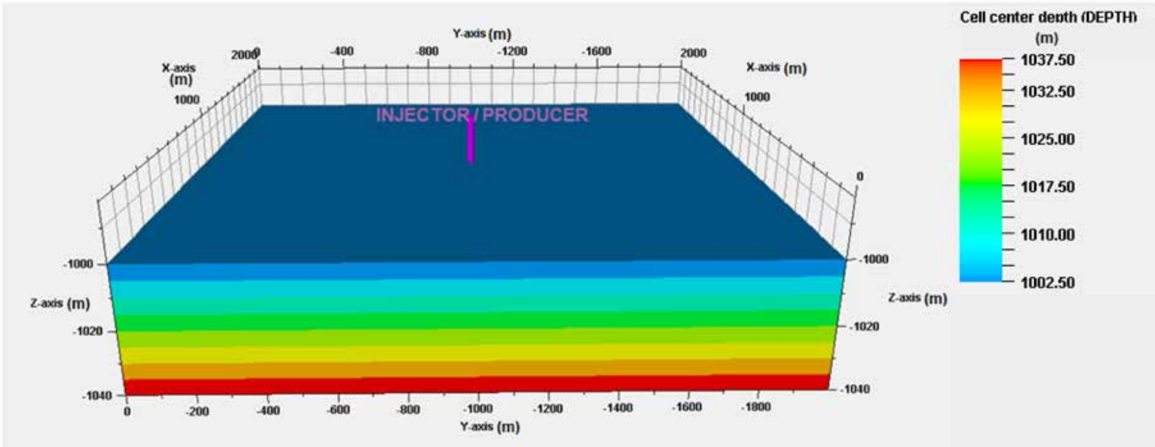

Figure 4—Numerical simulation domain showing the depth of the reservoir. The vertical exaggeration is 10.

A vertical well serves as both the injection and withdrawal well and is perforated in the top 15 m of the reservoir. The injection and withdrawal rates are defined by the cycles.

We determined the density of methane (CH_4) and hydrogen (H_2) using a generalized formulation of the Peng–Robinson equation of state (Schlumberger, 2016). We obtained binary interaction coefficients (BIC) from Qian et al. (2013). As part of the ECLIPSE E300 software, gas-phase viscosities were computed using the Lorentz-Bray-Clark (LBC) correlation. With the parameters used in this study (Table 4), the densities obtained for reservoir conditions are within 1.9% and 2.2% of the values given in Lemmon et al. (2021) for H_2 and CH_4, respectively. Viscosity values for H_2 and CH_4 deviated up to 12.2% and 1.5% respectively from those given in Lemmon et al. (2021); however, these values are still within the uncertainty range given in Lemmon et al. (2021), that are 15% and 2% for H_2 and CH_4, respectively.

The relative permeability used in the study was determined from the work by Yekta et al. (2018) and was input as tables into the simulation. The simulation included gas dissolution in connate water. The solubility of hydrogen in water at 43 ºC was taken from Wiebe and Gaddy (1934), while the solubility of methane in water at 43 ºC was taken from Culberson and McKetta (1951).

The reservoir pressure was considered depleted to 80 bar at a reference depth of 1000 m, about 20 bar below the hydrostatic pressure for that depth. The caprock was assumed to be tight against the stored $H_2$and CH_4 and was thus represented in the simulation as a no-flow boundary. Diffusion within the gas phase was neglected, and no geomechanical effects were considered during the simulation. Moreover, no degradation of hydrogen via reaction was incorporated.

Because this model was not designed for a specific field or reservoir, we set the maximum and minimum allowable BHPs to 120 bars and 30 bars at the reservoir top depth. The specified upper BHP limit corresponds to typical overbalance margins used during drilling, ranging from 20 bar to 35 bar (Kastor & Letbetter, 1974). In case of a violation of the BHP limits, the simulator automatically adapts the well flow rate until the pressure is within the specified range. The minimum allowable BHP was set to allow for a 10-bar pressure drop between the bottom hole and the well head, assuming a tubing head pressure (THP) of 20 bar. The wellbore had a nominal diameter of 0.3 m. Skin effects on the well flow rates were neglected.

We initialized the model by enumeration through specifying an average gas saturation of 0.3. Once the model equilibrates, gravity segregation occurs with high gas saturation at the top of the reservoir. This results in 30% of the reservoir thickness occupied by the reservoir gas and the remaining 70% occupied by water.

Results and Discussion

Hydrogen volumes and storage cycle

Figure 5 shows the hydrogen volume generated using the PEM electrolyzer considering the two extremes in efficiencies, i.e., 50 and 83 kWh/kgH_2, and converting the mass to volumes using the density of hydrogen at 15. 6 °C and 1 atm (0.08504 kg/m^3).

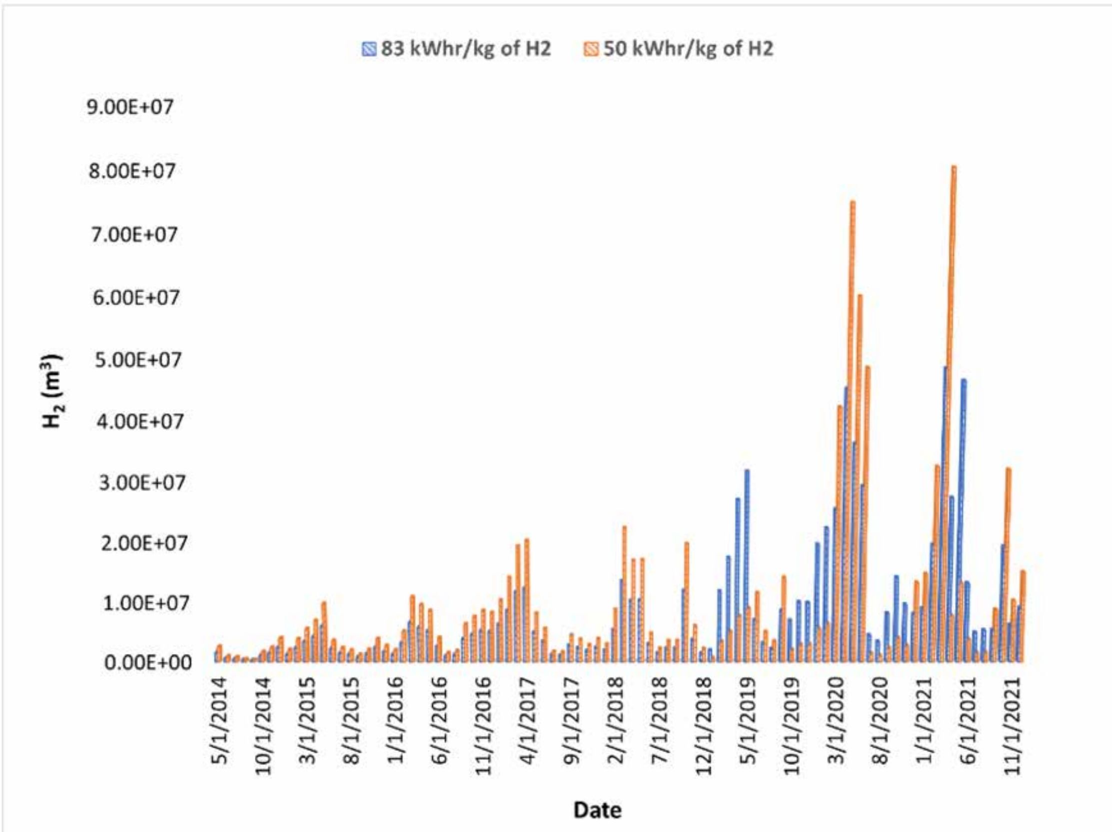

Figure 5—The hydrogen volume from the mass of hydrogen generated using the PEM electrolyzer. The extremes of the efficiencies, 50 and 83 kWh/kgH_2, were considered.

We fit a linear equation to the annual curtailed energy over time and got a relationship to forecast future curtailments as shown in Fig. 6. Using the trendline shown in Fig. 5, the predicted wind and solar curtailment for 2022 is about 1.3×10^6 MWh, equivalent to 1.86×10^8 or 3.09×10^8 m^3 of hydrogen at 15.56 °C and 1 atm, depending on the PEM efficiency of 83 or 50 kWh/kgH_2, respectively. We then define the storage volumes and cycle for 2022 and 2023 using the optimistic PEM efficiency of 50kWh/kgH_2 as shown in Figure 7.

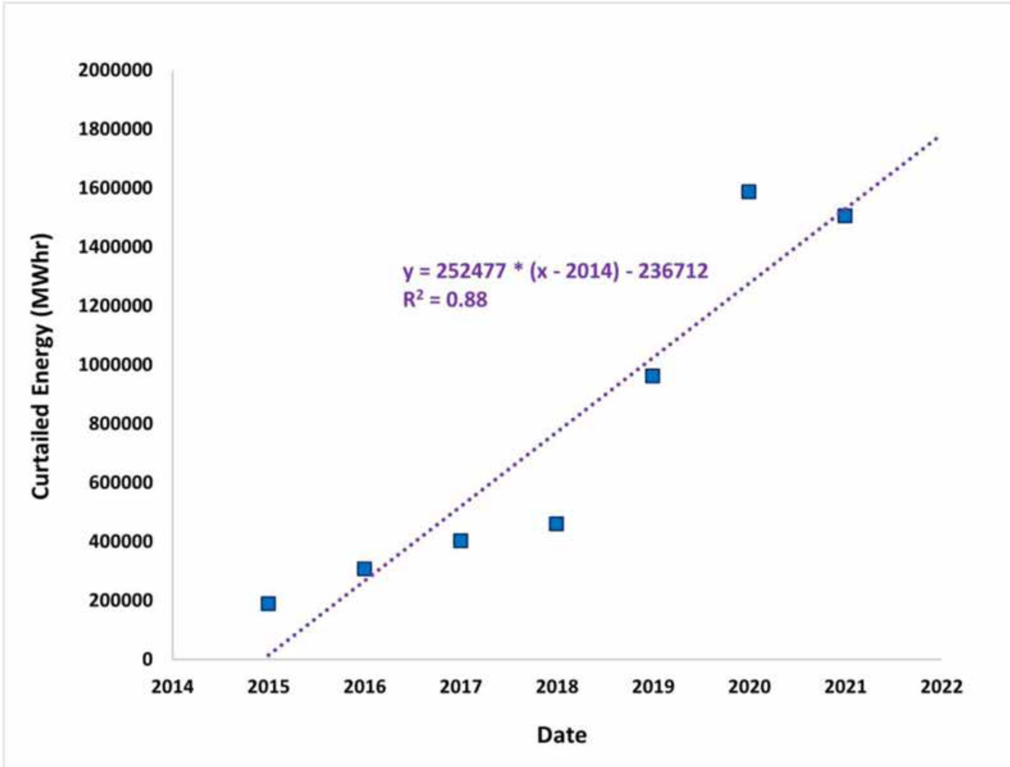

Figure 6—Linear fit to generate an expression for the relationship between the curtailed energy and time.

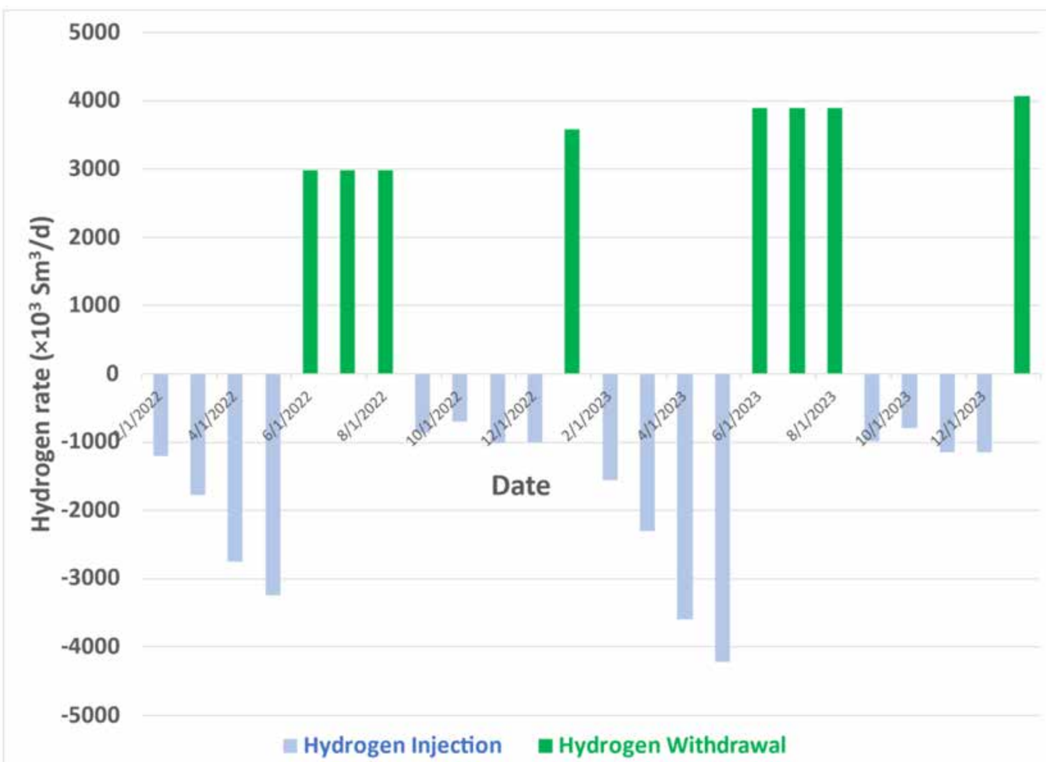

Figure 7—Hydrogen injection (blue) and withdrawal (green) rates forecasted for years 2022 and 2023.

Screening and Ranking of Potential Storage Sites

We applied the stage 1 screening criteria to identify the most suitable sites for underground hydrogen storage. Of the 175 oil & gas fields and 7 underground gas storage (UGS) sites, 35 fields passed the stage 1 screening. We then applied the scoring system shown in Table 2 to score each of the fields on their suitability for underground hydrogen storage. Of the 9 criteria listed in Table 2, we only ranked the sites based on seven parameters due to data availability. The seven parameters include permeability thickness (or flow capacity), storage capacity at STP, porosity, current reservoir pressure, reservoir dip, reservoir structure, and geothermal gradient.

Table 5 shows the top-ten scoring sites from the stage 2 ranking. Appendix A has the list of all the sites that were ranked. These top 10 ranking sites altogether have an estimated storage capacity of 203.5 million metric tonnes of H_2 at 30 bar and 40 °C.

Table 5—Top ranking sites from stage 2 ranking of sites for underground hydrogen storage

Field Name	Top Depth of Formation (m)	Mean Volume (million metric tonnes of H_2 at 30 bar) (Mt)	Total Score (weighted)	Rank
RIO VISTA GAS	1,372	146.57	38.0	1
SYCAMORE GAS	838	4.76	34.3	2
PUTAH SINK GAS	1,692	7.06	33.3	3
SUTTER CITY GAS	518	8.22	33.3	3
WILD GOOSE GAS	762	26.62	33.0	5
OAKLEY, S. GAS	2,384	6.00	31.3	6
PRINCETON GAS	661	1.74	31.3	6
BRENTWOOD	1,073	1.29	30.8	8
BUTTE SLOUGH GAS	553	0.86	30.5	9
WILLOW PASS GAS	549	0.41	29.5	10

Figure 8 shows all the sites in northern California that passed stage 1 screening on a GIS map. The sites are color coded with respect to how they ranked in stage 2. The top ten ranking sites are colored green, the next 12 sites are colored yellow, and the remaining 13 sites that ranked low are colored red. In Fig. 8, we show the names of only the top ten ranking sites.

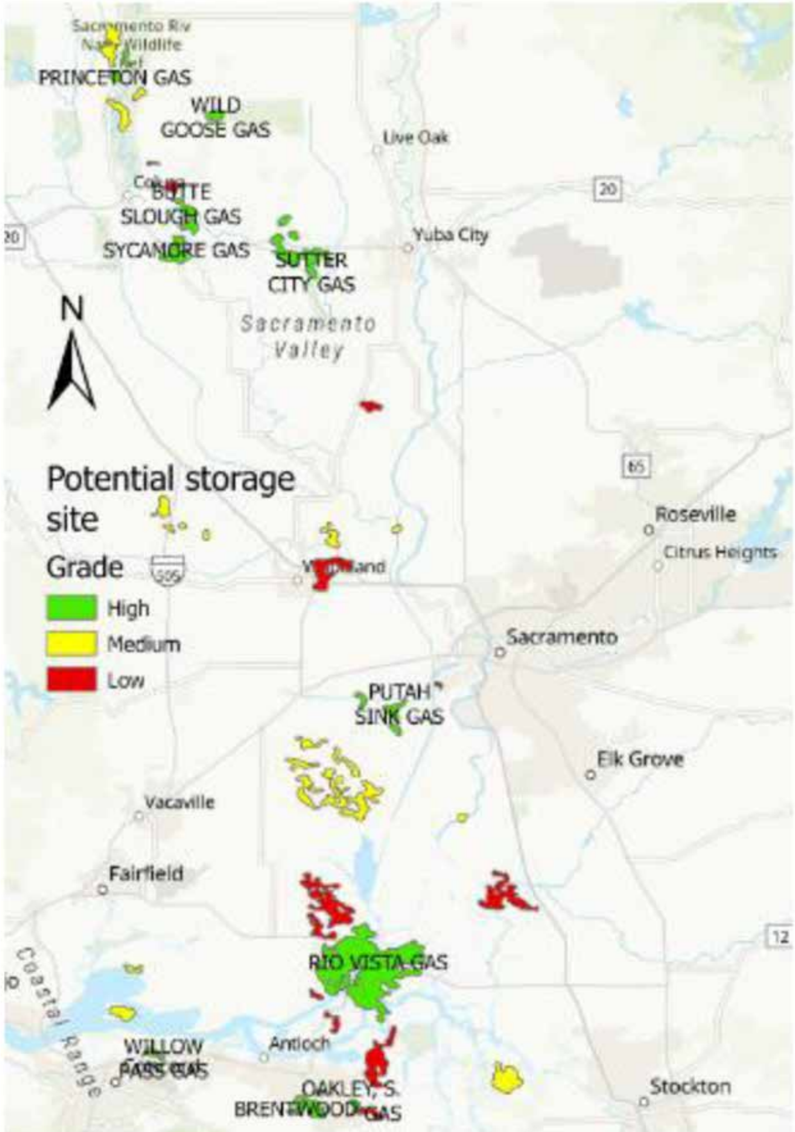

Figure 8—GIS Map of the fields that passed the stage 1 screening criteria.

Estimating the process efficiency

To calculate the energy content of the withdrawn hydrogen, we considered the lower heating value (LHV) or net heat of combustion. According to the thermodynamic properties of hydrogen given in the National Academies Press (NAP, 2004), the LHV of 1 kg of hydrogen is 33.3 kWh. The conversion of hydrogen back into electricity can be done using gas turbines, internal combustion engines, and large-scale combined cycle power plants. They have various efficiencies ranging from 30% for gas turbines (Mike Steilen, 2015) and up to 64% for large-scale combined cycle plants (GE Gas Power, 2022).

We estimated the overall process efficiency by comparing the amount of curtailed energy that was converted to hydrogen for storage to the amount of energy produced when hydrogen was extracted and used to generate electricity. This efficiency was computed on a cycle-by-cycle basis. The results are presented in Table 6 based on a 64% gas turbine efficiency. The cumulative volumes are taken from Fig. 9 computed for the hypothetical storage reservoir. We also include simulation results for a reservoir with a 10° dip to determine how a different reservoir structure impacts the overall efficiency. The results are presented in Table 7.

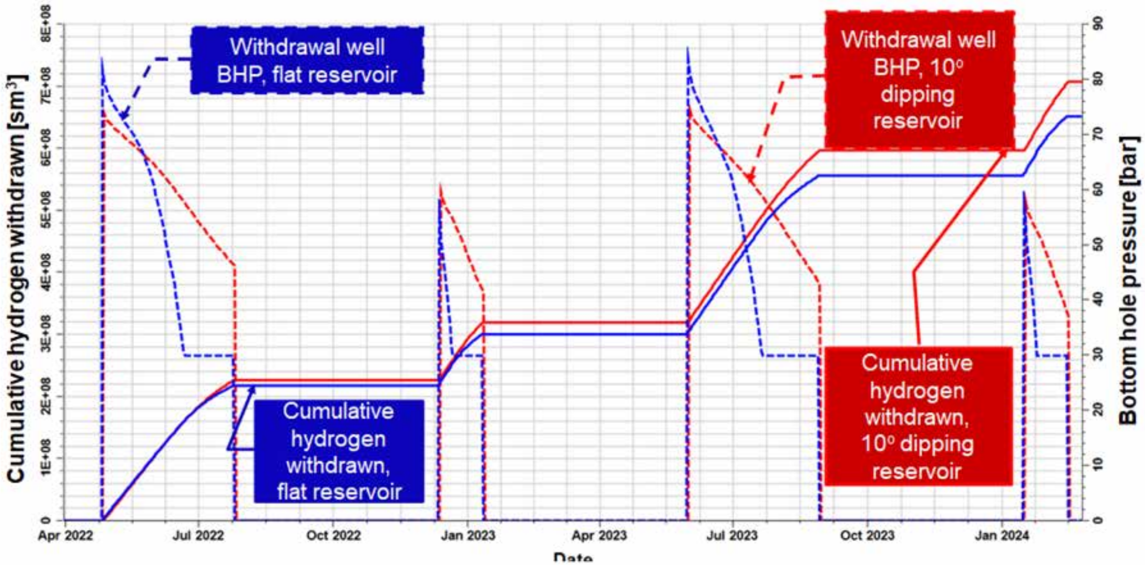

Figure 9—Cumulative hydrogen withdrawn for each cycle considering a flat reservoir and a reservoir dipping at 10°.

Table 6—Estimated overall power-to-hydrogen-to-power efficiency for underground hydrogen storage considering a 64% turbine efficiency.

Cycle	Cumulative Hydrogen Injected (× 10^8 sm^3)	Cumulative Hydrogen Withdrawn (× 10^8 sm^3)	Withdrawal Efficiency (%)	Equivalent Energy LHV (× 10^3 MWh)	Estimated Energy at 64% turbine efficiency (× 10^3 MWh)	Curtailed Energy converted to Hydrogen (× 10^3 MWh)	Overall Process Efficiency (%)
1	2.69	2.18	**81**	619	396	1143	**35**
2	1.07	0.83	**78**	235	150	457	**33**
3	3.08	2.55	**83**	723	463	1929	**24**
4	1.23	0.96	**78**	272	174	592	**29**

Table 7—Estimated overall power-to-hydrogen-to-power efficiency for underground hydrogen storage considering a 64% turbine efficiency and a 10° dipping reservoir.

Cycle	Cumulative Hydrogen Injected (× 10^8 sm^3)	Cumulative Hydrogen Withdrawn (× 10^8 sm^3)	Withdrawal Efficiency (%)	Equivalent Energy LHV (× 10^3 MWh)	Estimated Energy at 64% turbine efficiency (× 10^3 MWh)	Curtailed Energy converted to Hydrogen (× 10^3 MWh)	Overall Process Efficiency (%)
1	2.69	2.28	**85**	645	413	1143	**36**
2	1.07	0.87	**81**	246	157	457	**34**
3	3.08	2.83	**92**	802	513	1929	**27**
4	1.23	1.11	**90**	314	201	592	**34**

The results on computing efficiency show overall process efficiency less than 40%. However, the hydrogen withdrawal efficiencies are high, above 75%. These results show that the main barrier to complementing renewable energy with underground storage of hydrogen in depleted reservoirs is not significantly on the withdrawal of hydrogen from the reservoir. The overall process efficiency being less than 40% demonstrates the need to improve efficiency at various stages of the conversion process. Improving the efficiency of electrolysis and power generation can be focus areas.

Conclusion and Future Work

We have assessed the potential of northern California's depleted fields for underground hydrogen storage. We used a screening and ranking set of criteria to identify fields that are most likely candidates for underground hydrogen storage. 35 fields were deemed suitable for underground hydrogen storage based on the screening criteria applied. The withdrawal efficiencies were above 75% based on the assumptions made for the numerical model. However, the overall power-to-hydrogen-to-power efficiencies were below 40%.

This study shows that northern California has sufficient capacity for underground hydrogen storage in depleted fields. The top 10 ranking sites altogether have an estimated storage capacity of 203.5 million metric tonnes of H_2 at 30 bar and 40 °C. The limitation on the overall process efficiency is not essentially dependent on the recovery of hydrogen, but on other processes involved in the conversion of renewable power to hydrogen, and converting hydrogen back to power.

We performed this study using data with significant uncertainty (such as reservoir pressure and permeability). It is imperative to have current and accurate values of the parameters to perform screening and scoring of the sites. Hence, future work should focus on reducing the uncertainty in the input data for screening.

The numerical reservoir model used in this study did not consider the reactions between hydrogen and the subsurface rock and fluid, geomechanical effects, and microbial activity. A more rigorous model that takes into account these processes will be considered in subsequent work, especially after additional data to characterize the sites have been gathered for stage 3.

Future work will examine the techno-economics of underground hydrogen storage combined with renewable energy generation. Such analysis may involve a cost analysis for green hydrogen to compare with the production cost of blue hydrogen, and the role of the Low Carbon Fuel Standard (LCFS) in the economics of green hydrogen generation.

Acknowledgment

We acknowledge the support of Southern Company, the Stanford Center for Carbon Storage, and the SUETRI-A (Sustainable Subsurface Engineering affiliates) program.

References

Andersson, J., & Grönkvist, S. (2019). Large-scale storage of hydrogen. *International Journal of Hydrogen Energy*, Volume **44**(Issue 23), 11901–11919.

Bracci, J., Okoroafor, E. R., Shrimali, G., Hennessy, E., Kim, T., Biddle Seamon, D., … Zoback, M. D. (2022). Fueling the California Mobility Market with Hydrogen from Natural Gas plus Carbon Capture and Storage. Stanford Natural Gas Initiative and Stanford Center for Carbon Storage.

California Department of Conservation (CA DOC). (2022). WellSTAR Data Dashboard, https://www.conservation.ca.gov/calgem/Online_Data/Pages/WellSTAR-Data-Dashboard.aspx.

California Division of Oil, Gas and Geothermal Resources (CA DOGGR). (1982) California Oil and Gas Fields, VolumeIII – Northern California. California Department of Conservation.

California ISO. (2022, January 10). *Managing oversupply*. Retrieved from California ISO: http://www.caiso.com/informed/Pages/ManagingOversupply.aspx

Callas, C., Saltzer, S. D., Davis, J. S., Hashemi, S. S., Kovscek, A. R., Okoroafor, E. R., … Benson, S. M. (2022). Criteria and Workflow for Selecting Depleted Hydrocarbon Reservoirs for Carbon Storage. *Applied Energy*.

Culberson, O. L., & McKetta, J. J. (1951). Phase Equilibria in Hydrocarbon-Water Systems III - The Solubility of Methane in Water at Pressures to 10,000 PSIA. *J Pet Technol* **3**, 223–226.

DOE/NETL. (2010). Assessment of hydrogen production with CO_2 capture. US DOE National Energy Technology Laboratory. In Baseline state-of-the-art plants (Vol. **1**).

EIA. (2021, August 24). California's curtailments of solar electricity generation continue to increase. Retrieved from Independent Statistics and Information US Energy Information Administration: https://www.eia.gov/todayinenergy/detail.php?id=49276

GE Gas Power. (2022, April 24). 9HA gas turbine. Retrieved from GE Gas Power: https://www.ge.com/gas-power/products/gas-turbines/9ha

IRENA. (2020). *Green Hydrogen Cost Reduction: Scaling up Electrolysers to Meet the 1.5#C Climate Goal*. Abu Dhabi: International Renewable Energy Agency.

Kastor, R. L., & Letbetter, S. C. (1974). Extra Increments of Pressure or Mud Weight Safety Factors Added During Well Killing Procedures Can Be Unsafe. Paper presented at the Fall Meeting of the Society of Petroleum Engineers of AIME, Houston, Texas.

Kim, T.W., Callas, C., Saltzer, S. D. and Kovscek, A. R. (2022a). Assessment of oil and gas fields in California as potential CO_2 storage sites, *International Journal of Greenhouse Gas Control*, **114**, 103579.

Kim, Tae Wook, Yaw, Sean, and Kovseck, A. R. (2022b). Evaluation of Geological Carbon Storage Opportunities in California and a Deep Look in the Vicinity of Kern County, Paper presented at the SPE Western Regional Meeting, Bakersfield, California, USA, April, doi: https://doi.org/10.2118/209340-MS

Lemmon, E. W., Bell, I. H., Huber, M. L., & McLinden, M. O. (2021). Thermophysical Properties of Fluid Systems. *NIST Chemistry WebBook, NIST Standard Reference Database Number 69*. (P. J. Linstrom, & W. G. Mallard, Eds.) Gaithersburg, MD: National Institute of Standards and Technology. Retrieved September 2, 2021

Lichner, C. (2020, March 21). *The weekend read: Hydrogen is getting cheaper*. Retrieved from PV Magazine: https://www.pv-magazine.com/2020/03/21/the-weekend-read-hydrogen-is-getting-cheaper/#:~:text=Compared%20to%20alkaline%20electrolysis%2C%20PEM,and%20delivers%20high%2Dquality%20gas.

Long J. C. S., Birkholzer, J.T., Mace, A.J. and Brady, S.E. (2018). *Long-Term Viability of Underground Natural Gas Storage in California*, California Council on Science and Technology (CCST).

NAP. (2004). *National Academic Press*. Retrieved from The Hydrogen Economy: Opportunities, Costs, Barriers, and R&D Needs: https://nap.nationalacademies.org/read/10922/chapter/21

National Energy Technology Laboratory (NETL). (2015). *The National Carbon Sequestration Database (NATCARB). National Energy Technology Laboratory*, https://edx.netl.doe.gov/dataset/natcarb-alldata-v1502.

Newman, G. H. (1973). Pore-volume compressibility. *J. Pet. Technol*., 129–134.

Okoroafor, E. R., Saltzer, S., & Kovscek, A. (2022). Towards Understanding Factors Relevant for Hydrogen Storage in Porous Media: Insights from Numerical Simulations. *International Journal of Hydrogen Energy*.

Panfilov, M. (2016). 4 - Underground and pipeline hydrogen storage. In W. P. Energy, R. B. Gupta, A. Basile, & N. T. Veziroğlu (Eds.), *Compendium of Hydrogen Energy (Vols. Volume 2: Hydrogen Storage, Transportation and Infrastructure*, pp. 91–115). Woodhead Publishing.

Press, R. J., Santhanam, K. S., Miri, M. J., Bailey, A. V., & Takacs, G. A. (2008). *Introduction to hydrogen Technology*. John Wiley & Sons.

Qian, J.-W., Jaubert, J.-N., & Privat, R. (2013). Phase equilibria in hydrogen-containing binary systems modeled with the Peng–Robinson equation of state and temperature-dependent binary interaction parameters calculated through a group-contribution method. *The Journal of Supercritical Fluids*, **5**, 58–71.

Ritchie, H., Roser, M., & Rosado, P. (2020). *CO# and Greenhouse Gas Emissions*. Retrieved from Our World In Data: https://ourworldindata.org/co2-and-other-greenhouse-gas-emissions

Schlumberger. (2016). *ECLIPSE Technical Description*. Version 2016.2.

Scholz, W. (1993). Processes for industrial production of hydrogen and associated environmental effect. *Gas Seperation & Purification*, **7**, 131–139.

Steilen, M., Jörissen, L. (2015). Chapter 10 - Hydrogen Conversion into Electricity and Thermal Energy by Fuel Cells: Use of H2-Systems and Batteries. *In P. T. Garche, Electrochemical Energy Storage for Renewable Sources and Grid Balancing* (p. 149). Elsevier.

Stetson, N. T., McWhorter, S., & Ahn, C. C. (2016). *Introduction to hydrogen storage (Vols. Volume 2:hydrogen Storage, Transportation and Infrastructure)*. (R. B. Gupta, A. Basile, & T. N. Veziroğlu, Eds.) Woodhead Publishing.

Tarkowski, R. (2019). Underground hydrogen storage: Characteristics and prospects. *Renewable and Sustainable Energy Reviews*, **105**, pp.86–94.

United States Environmental Protection Agency(US EPA). 2022. 2020 Emission & Generation Resources Integrated Database (eGRID 2020). https://www.epa.gov/egrid/download-data

Wiebe, R., & Gaddy, V. L. (1934). The Solubility of Hydrogen in Water at 0, 50, 75 and 100° from 25 to 1000 Atmospheres. *J. Am. Chem. Soc.*, **56** (1), 76–79.

Yekta, A. E., Manceau, J. C., Gaboreau, S., Pichavant, M., & Audigane, P. (2018). Determination of hydrogen-water relative permeability and capillary pressure in sandstone: application to underground hydrogen injection in sedimentary formations. *Transport in Porous Media*, 333–356.

Zivar, D., Kumar, S., & Foroozesh, J. (2020). Underground hydrogen storage: A comprehensive review. *International Journal of Hydrogen Energy*, **46**(45), 23436–23462.

Appendix A

Details of Sites that passed the Stage 1 Screening

Field Name	Top Depth of Formation (m)	Mean Volume (million metric tonnes of H_2 at 30 bar) (Mt)	Total Score (weighted)	Rank (weighted)
RIO VISTA GAS	1,372	146.57	38.0	1
SYCAMORE GAS	838	4.76	34.3	2
PUTAH SINK GAS	1,692	7.06	33.3	3
SUTTER CITY GAS	518	8.22	33.3	3
WILD GOOSE GAS	762	26.62	33.0	5
OAKLEY, S. GAS	2,384	6.00	31.3	6
PRINCETON GAS	661	1.74	31.3	6
BRENTWOOD	1,073	1.29	30.8	8
BUTTE SLOUGH GAS	553	0.86	30.5	9
WILLOW PASS GAS	549	0.41	29.5	10
RYER ISLAND GAS	1,448	20.86	29.5	10
MERRITT ISLAND GAS	2,256	0.66	29.0	12
RIO JESUS GAS	753	0.52	28.5	13
COMPTON LANDING GAS	616	0.33	28.0	14
CACHE SLOUGH GAS (ABD.)	1,442	1.96	27.8	15
DUNNIGAN HILLS GAS (ABD.?)	747	0.63	27.5	16
GREENWOOD, S. GAS	430	0.09	27.5	16
MCDONALD ISLAND GAS	1,591	26.77	27.5	16
VERNALIS GAS	1,158	11.92	26.5	19
MILLAR GAS	1,398	14.75	26.5	19
BOUNDE CREEK GAS	1,128	4.43	25.8	21
SUISUN BAY GAS	1,265	5.96	25.8	21
LATHROP GAS	2,105	40.07	25.5	23
THORNTON-WALNUT, W. GROVE GAS	1,085	14.19	25.0	24
SHERMAN ISLAND GAS	1,859	1.16	23.8	25
TRACY GAS	1,189	1.30	23.8	25
LINDSEY SLOUGH GAS	2,126	25.47	23.0	27
GREENS LAKE GAS (ABD.)	975	0.05	22.5	28
BUTTE SINK GAS	610	0.55	22.0	29
DUTCH SLOUGH GAS	2,195	9.82	21.8	30
BRENTWOOD, E. GAS	2,438	5.06	20.3	31
DURHAM GAS	649	0.50	20.0	32
ROBBINS GAS	2,164	3.78	19.8	33
LATHROP, SE. GAS (ABD.)	2,167	0.01	19.0	34
CROSSROADS GAS	1,265	2.56	17.8	35